Analysis of electroluminescence and infrared thermal images of monocrystalline silicon photovoltaic modules after 20 years of outdoor use in a solar vehicle

I. Berardone[a,1], J. Lopez Garcia[b], M. Paggi[a]

[a]*IMT School for Advanced Studies Lucca, Piazza San Francesco 19, 55100 Lucca, Italy*
[b]*European Commission, DG JRC, Directorate C-Energy, Transport and Climate, Energy efficiency and Renewables Unit, Via E. Fermi 2749, 21027 Ispra (VA), Italy*

Abstract

Infrared (IR), under forward bias and under illuminated condition, and electroluminescence (EL) are the most employed non-desctructive techniques to monitor performance of photovoltaics (PV) modules. The application of these two techniques have advantages and drawbacks and a combined use has not been made extensively. With this purpose, we performed a quantitative comparison of EL and IR images of monocrystalline PV modules after 20 years of outdoor exposition and use. The proposed methodology relies in the analysis of frequency histograms of IR and EL images. Results provides local information on PV modules state, useful to distinguish disconnected cell interconnect, humidity corrosion, and broken fingers in highly damaged solar cells. This method contributes and supports to the current knowledge of IR and EL imaging techniques used to assess different forms of damage in monocrystalline silicon PV modules. Moreover, it could contribute to the future draft technical specification IEC 60904-13 for EL.

Keywords: electroluminescence, thermal infrared imaging, outdoor ageing, solar vehicle, crystalline silicon photovoltaics, image analysis.

Email addresses: `irene.berardone@imtlucca.it` (I. Berardone), `Juan.LOPEZ-GARCIA@ec.europa.eu` (J. Lopez Garcia), `marco.paggi@imtlucca.it` (M. Paggi)

1. Introduction

Operation and Maintenance (O&M) costs of photovoltaics plants are connected to performance monitoring and quality. An appropriate monitoring can reduce O&M costs of photovoltaics and, for this reason, the scientific community collects and analyzes data on PV performance and failures to study and understand challenges involved in damage phenomena. In this framework, IR thermography and EL are the most widely used monitoring techniques for quality control of PV modules. These two optical techniques provide real-time two-dimensional images and detect type of defects, malfunctioning, or even failures.

EL imaging is a high-resolution characterization method that provides a map of the voltage drop from a point to another over the solar cells, which is typically normalized in the range from 0 to 255 (Köntges et al., 2011; Paggi et al., 2014, 2016). Voltage drops are usually caused by defects or cracks, which induce a localized additional resistance. Furthermore, EL images visually detects also intrinsic (grain boundaries, dislocation, shunts or process failures) and extrinsic defects (cracks, interrupted contacts and TCO corrosion for thin-films). In the EL test, modules operate under forward bias like a light emitting diode (LED). Excitation current can be lower or equal to I_{sc}. The electroluminescence emission is due to radiative interband recombination of charge carriers (near-IR in the range from 300 up to 1000 nm, depending on the semiconductor type). A disadvantage of the EL techniques relies on its test condition, that requires dark environment, thus confining mostly to the lab. Recently, however, EL techniques made advances also in outdoor testing and in daylight conditions (Mertens et al., 2015; Kropp et al., 2017), thanks to the introduction of shrouds to cover the module, cameras able to work also in nearly dark environments at sunsets or at twilight, and lock-in technologies. Although in-field EL inspection techniques still has limits (i.e. power supply and module orientation), its employment is gradually growing, see e.g. (Muehleisen et al., 2018) for notable applications to hailstorm damages on PV plants. So far, production rates for EL data up to 1 MWp in just one night have been reported, especially with the use of drones (Koch et al., 2016).

Compared to EL, IR thermography is a cost-effective and time saving method. It is able to detect mostly general electric problem (i.e. electrical disconnections, bypassed strings, faulty soldering and short-circuited cells) (Buerhop et al., 2011). IR thermography can be performed in dark or illumi-

nated conditions (Zamini et al., 2012). The dark IR procedure requires that a forward voltage is applied to the module, similarly to EL. Otherwise, illuminated IR thermography is analogous to luminescence, where the current flowing through cells increases PV module temperature.

Although a correlation between temperature increase and power reduction of a module has been thoroughly demonstrated (Ebner et al., 2010), a quantitative interpretation of IR images is still under debate. A large number of studies have analyzed EL and IR techniques (Zamini et al., 2012; Ebner et al., 2015b, 2010; Breitenstein et al., 2008; Gade et al., 2015; Würfel et al., 2007; Bothe et al., 2006, 2007; Hinken et al., 2007; Haunschild et al., 2009; Lopez et al., 2015) and in some cases including also photoluminescence (Ebner et al., 2013, 2015b,a), but an overall discussion on the potential use of IR and EL techniques to detect the wide range of damage scenarios affecting PV modules in the field has not yet been reported. The common target of studies on EL is the determination of physical proprieties of solar cells, such as local effective diffusion length l_{eff} (Würfel et al., 2007), carrier collection length l_{c} (Bothe et al., 2007), local junction voltage (Gade et al., 2015), series resistance (Hinken et al., 2007). Zamini et al. (2012) proposed preliminary qualitative comparisons between EL and IR images for crystalline silicon and thin film technologies, further extending the investigation in a range of selected articles (Ebner et al., 2013, 2015a), finding important spatial correlations between dark IR measurement and EL images for thin-film solar cells.

To understand challenges involved in failure detection and to quantitatively compare IR and EL techniques, we propose a statistical analysis of the data extracted from EL, dark-IR and illuminated IR imaging of crystalline silicon PV modules. The importance and novelty of the results relies in the possibility to implement the identified correlations in machine learning software for the automatic inspection of PV modules in real time. This can be very important for a fast and accurate detection and classification of the various forms of damage affecting PV modules durability and consequently reduce O&M costs.

2. Methods and materials

Four crystalline silicon PV modules manufactured in the mid-1980's were characterised by EL and IR imaging techniques. In particular they were installed on a solar car (Mazzieri model, equipped with an electric motor of

Figure 1: Mazzieri solar car and modules disposition on it.

7 cV and a maximum speed of 70 km/h) and exposed to outdoor condition for 20 years. They were named IY41, IY42, IY43 and IY44, details on module manufacture and characteristic are also summarized in Tab.1.

Table 1: List of PV modules analyzed in the present study.

Module	Producer	Model	# cells	Year outdoor
IY41	BP	1242	36	20
IY42	Arcosolar	M75	33	20
IY43	Arcosolar	M75	33	20
IY44	Arcosolar	M75	33	20

Three modules (IY42, IY43, IY44) were placed on the roof and the one on the bonnet (IY41) of the car. They were connected to a battery. The disposition of module on the solar car was the following: module IY41 had a tilt angle of 12°, IY42 and IY44 of 8°, while IY43 was installed horizontally on the roof (see Fig. 1).

This vehicle was a service car at Joint Research Center (JRC) in Ispra, in the North of Italy. Ispra is at 220 m above sea level and belongs to moderate subtropical climate zone (temperature excursion during the year from -10 °C

up to +35 °C, relative humidity $\leq 90\%$ (Strahler et al., 1981)). The solar car was driven in this region for about 20 years, without module cleaning.

In 2015, the PV modules were removed from the car and subjected, without being cleaned, to visual inspection and electrical tests. Afterwards, modules were cleaned manually for 10 minutes with a soft sponge, a standard commercial glass cleaning detergent and finally dried with a cloth. The cleaned modules were characterized at JRC center through visual characterization, I-V measurement, electroluminescence and infrared thermography.

In 2015, I-V curves were measured using the Pasan IIIB flash simulator, having a flash duration of 10 ms. This system presents some differences compared to the one used to characterize the IY41 module in 1988, which had a shorter flash duration with an I-V curve sweep of 1.5 ms. Also the reference cells used for the measurements in 1988 and in 2015 were different. It has been previously reported the potential difference introduced in the measurements by the setup used in the 1980's and the one used in 2015 at the ESTI laboratory (Lopez-Garcia et al., 2015). Since there are no initial measurements available of the stored modules IY45, IY46 nor a reference module similar to IY41, the results of the cited work with similar crystalline silicon modules manufacturer in the same date are extrapolated. It was observed that part of the differences in measurements found using the two setups can be attributed to the enhanced temperature control that was implemented between the 1980's and 2015 and to the different spectrum of the two simulators. Another factor that had an influence was the different reference cell used to measure the modules in 1980's and in 2015. Given these differences, the measurements performed in 1980's and in 2015 were found to be of similar order, therefore giving confidence that the changes measured after long-term exposures are the result of ageing.

Electroluminescence images were performed with a Sensovation digital camera SVSB14-M under forward bias with a current equal to I_{sc} and exposure time of 300 s.

Original dark IR images of the PV modules were taken at JRC using a Fluke Ti55 camera under forward bias, with a current equal to I_{sc}. Illuminated IR images were taken under continuous illumination (~ 1000 W/m^2), provided by a steady state solar simulator and short circuited with a 15Ω resistance. To perform a statistical analysis of EL and IR signal, we modified the initial images reducing distortions in IR images.

According to the International Energy Agency classification reported in (Köntges et al., 2014), we identified and classified defective cells of the an-

alyzed modules from the EL images. After this EL-based classification, we analyzed IR and EL signals through a user defined subroutine written in MATLAB. Preliminary and automatic operations of the developed subroutine involve the extraction of all the individual solar cells and the conversion of the signals into multi-dimensional matrices of real numbers. For IR images, the multi-dimensional matrix collects the x and y position coordinates of each pixel and the corresponding RGB channels. Each channel is normalized in the range from 0 to 1.

To synthetically characterize the information contained in the RGB channels, these data were also converted to real values ranging from 255 (code number for blue) to 16711680 (code number for red) and then transformed in a temperature scale, of easy visualization to draw thermal maps for each module under forward bias or illumination. Similarly, for EL images, a three-dimensional matrix is introduced by collecting the x and y coordinates of each pixel and the corresponding EL signal ranging from 0 to 255. Such a range has been normalized from 0 to 1 for easy of visualization.

The first operation for the statistical analysis of the data was the computation of frequency histograms for R, G, B and EL signal (using 50 bins for each image). Quantity of interest were the position of the histogram interval, with occurrences higher than a prescribed minimum tolerance. To minimize the noise this threshold was set equal to the 80% of the average of the occurrences. This procedure is applied to each cell and the interval position depends both on defect type and on module condition.

3. Results and discussion

3.1. Visual characterization

All the modules were not cleaned after installation on the car indeed, visual characterization showed soiling in all modules (Fig. 2). In the images presented in this study, each cell is identified with a code composed by module name, a letter and a number. The letter identifies the row, instead the number identifies the column of each defective cell. The quasi-horizontal mounting configuration caused a uniform distribution of soiling whereas, modules with low tilted angle showed a more pronounced soiling in the lower part of the module, close to the frame. Visual characterization highlighted several types of damage as delamination (close to the cell interconnect ribbons and over the cell, respectively), cracked cells, discoloration of cells, interconnect ribbons and yellowing of the center or whole cells.
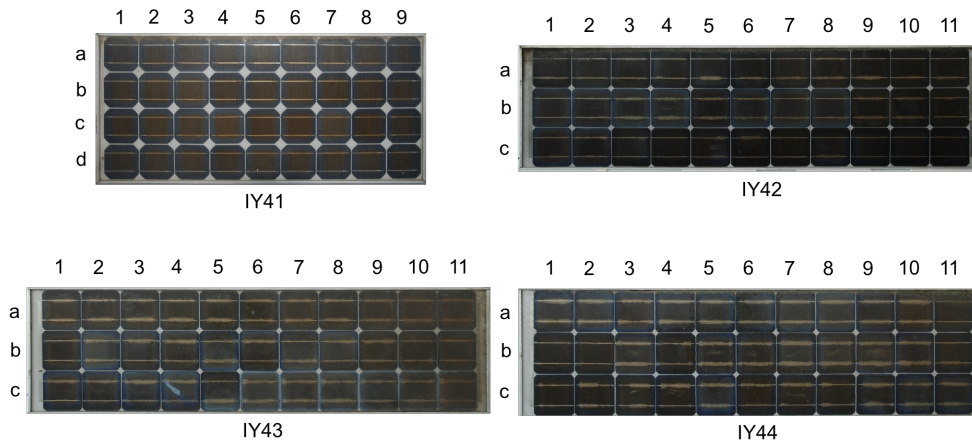
Figure 2: Visual characterization of the four modules IY41, IY42, IY43 and IY44.

3.2. Electrical characterization

I–V measurements were performed, before and after cleaning, after 20 years of outdoor exposure. Before cleaning, Arcosolar I-V curves present kinks at low voltage, absent in the case of the module stored in the basement taken as reference (orange line), see Fig. 3. This can be attributed to the soiling and to a non-uniform shading. Generally, I–V kinks due to non-uniform shading (i.e. soiling) are reversible and disappear after manual cleaning or major rainfall events (Schill et al., 2011; Dolara et al., 2013; Schill et al., 2015). Otherwise, kinks in modules IY42 and IY44 are still evident after cleaning, and this suggests the presence of additional problem as a higher level of damage.

Fig. 4 shows three I–V curves for IY41 module: in 1988 (red line), in 2015 before (blue line) and after cleaning (green line). In this case, the kink at low voltage is present in the blue curve, probably due to soiling, and it disappears after cleaning.

The electrical parameter of Arcosolar and BP modules are summarized in Tab. 2 and Tab. 3. Variations in electrical parameters before and after cleaning of the whole set of modules are reported in Tab. 2.

The increase in $P_{\max}$ after cleaning (except in module IY43) is greater than usual values reported for long-term soiling, around 9.8% (Lopez-Garcia et al., 2016). This increase is the result of I_{sc} and I_{mpp} growth. Otherwise, module IY43 shows a decrease in $P_{\max}$ (-9.70%) and FF (-34.1%) after

7
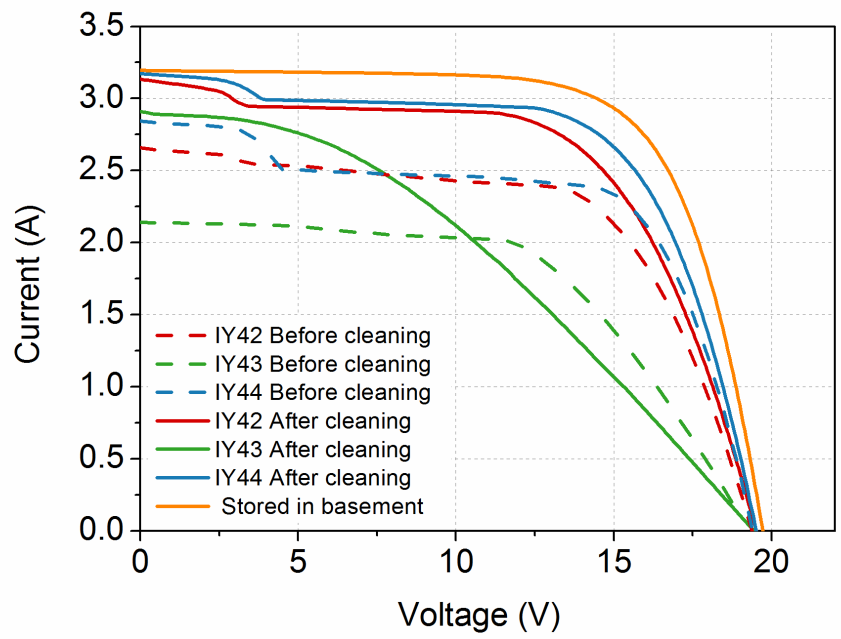
Figure 3: I-V measurement for IY42, IY43 and IY44 before and after cleaning.
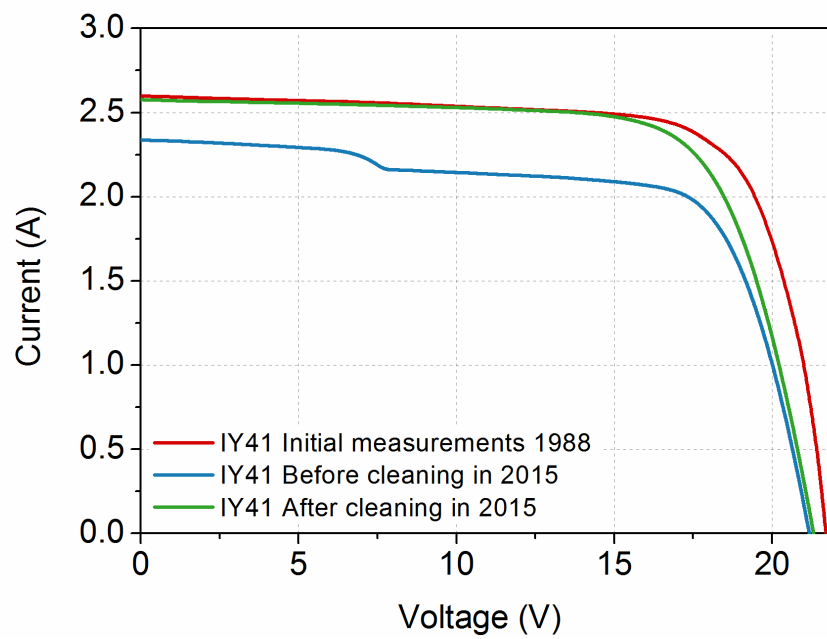
Figure 4: I-V measurement for IY41 before the connection to the car in 1988 (red line) and 2015, before (blue line) and after cleaning (green line).

Table 2: Difference between electrical parameters measured before and after cleaning in 2015.

Module	ΔI_{sc} (%)	ΔV_{oc} (%)	ΔP_{max} (%)	ΔFF (%)	ΔI_{mpp} (%)	ΔV_{mpp} (%)
IY41	10.20	0.63	14.98	3.69	17.16	-1.86
IY42	17.20	0.70	13.77	-4.21	15.05	-1.11
IY43	36.01	0.75	-9.70	-34.10	5.99	-14.81
IY44	11.06	0.58	13.63	1.71	16.79	-2.71

manual cleaning. That may be the effect of broken cells or fingers already present in the module, covered by soiling.

Tab. 3 reports the difference in a part of electrical parameters (I_{sc}, V_{oc}, P_{max}) measured before installation in 1988 and after cleaning in 2015, for all the modules. Arcosolar modules show a higher degradation ΔP_{max}, i.e. IY43 reaches the highest value (-55.26%), that evidences again the presence of damages. Instead, module IY41 has low difference in P_{max} (-4.69%), I_{sc} (-0.90%) and V_{oc} (-1.79%), it proves that IY41 has a low damage intensity.

Table 3: Difference between electrical parameters measured in 1988 and 2015.

Module	ΔI_{sc} (%)	ΔV_{oc} (%)	ΔP_{max} (%)
IY41	-0.90	-1.79	-4.69
IY42	-10.18	-11.30	-23.02
IY43	-16.61	-11.70	-55.26
IY44	-16.14	-11.31	-16.91

3.3. Electroluminescence and infrared characterization

Measurement condition for EL images (see Fig. 5) was the same for all modules, thus resulting EL intensity is related to minority carried diffusion length (Fuyuki et al., 2007). EL image of IY41 presents darker cells in the bottom of the module, close to the soiled edge. Other defects are sucker handling (2d, 3d, 4d, 5d), striation rings (9c, 1d), poor ribbon soldering (1a, 6b, 9b), finger interruption. EL images of IY42 and IY43 show brighter spot close to the busbar or cell interconnect ribbons, and the overall EL intensity is very low. Reasons for brighter spots are contacting problems. The cell
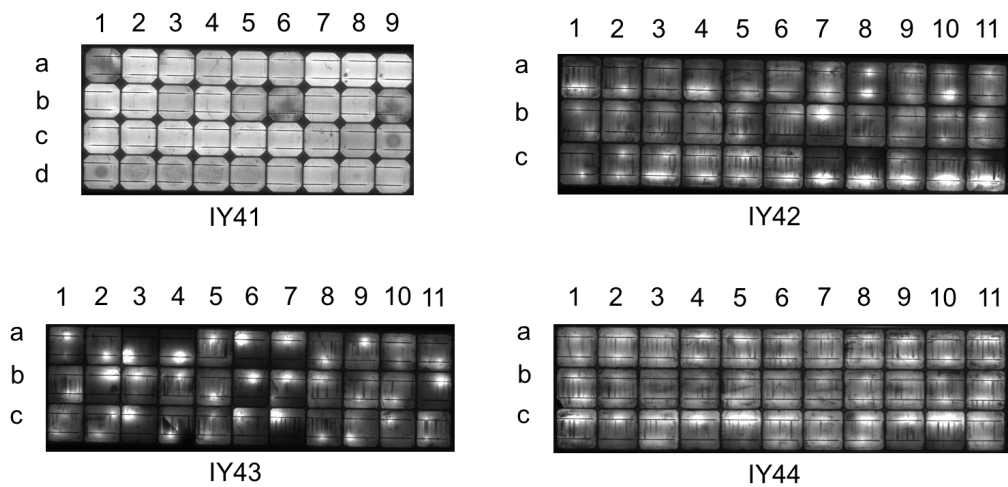
Figure 5: Electroluminescence images of the for modules IY41, IY42, IY43 and IY44.

with the lowest intensity shows a crack, that electrically disconnects a part of the cell (4c in IY43). IY44 has a low EL intensity and the a high numbers of finger interruptions.

From the analysis of the EL signal, damaged cells can be classified depending on the type of defect (see Fig. 6), according to the classification in (Köntges et al., 2014). The first column of the table in Fig. 6 is reporting code of the defect, followed by the nomenclature, the EL image of a corresponding solar cell and finally in the last column the module belonging to each class of defect.

The severity of defects increases from SR to DCL based on the brightness of the EL image of the cells that becomes dimmer and dimmer from SR to DCL. IR images under forward bias condition have spots with higher temperature, as shown in Fig. 7. One is present in module IY41, two in IY42, three hot spot in IY43 and a brighter line in the bottom of IY44, corresponding to higher resistivity along the interconnect ribbons. Illuminated IR images, on the other hand, do not show particular defect point (see Fig. 8).

We adopted the method described in Sec.2 to compute the thermal maps starting of the IR images. Thermal maps of IR under forward bias show spots with higher temperature in correspondence of a part of defects visible in the EL images (Fig. 9). On the other hand, thermal maps corresponding to
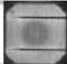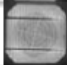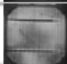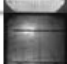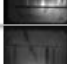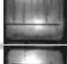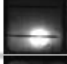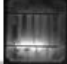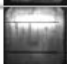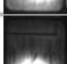
Module	Name		Module / cells
SR	Striation Ring		IY41
SH	Sucker handling		IY41
CFb	Contact forming		IY41-IY44
HC1	Humidity corrosion in a low damaged solar cell		IY41
HC2	Humidity corrosion in a high damaged solar cell		IY43
CC1	Cross Crack in a low damaged solar cell		IY43
CC2	Cross Crack in a high damaged solar cell		IY41
Fc	Finger interruption C		IY43, IY44
DCIxs1	Disconnected cell interconnect (spot) in a high damaged solar cell		IY43
DCIxs2	Disconnected cell interconnect (spot) in a medium damaged solar cell		IY42
DCIxs3	Disconnected cell interconnect (spot) in a low damaged solar cell		IY44
DCIxxs1	Disconnected cell interconnect (spot) in a low damaged solar cell		IY42, IY43
DCIxxs2	Disconnected cell interconnect (spot) in a high damaged solar cell		IY44
DCIxxl1	Disconnected cell interconnect (line) in a high damaged solar cell		IY43, IY42 (1A)
DCIxxl2	Disconnected cell interconnect (line) in a low damaged solar cell		IY42
DCIxxl3	Disconnected cell interconnect (line, extended to a full busbar)		IY44
DCIxxxl1	Disconnected cell interconnect (line) in a high damaged solar cell		IY42 (10C, 9C,3C)
DCIxxxl2	Disconnected cell interconnect (line) in a low damaged solar cell		IY43, IY42 (8C, 11C, 7C)
MC	Micro-crack C (isolating part)		IY43

Figure 6: List of defect classes considered, adapted from (Köntges et al., 2014).
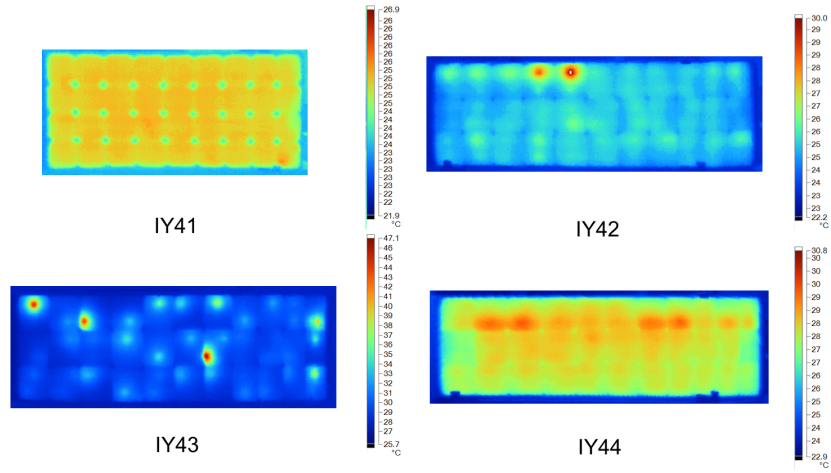
Figure 7: Dark infrared thermography images for modules IY41, IY42, IY43 and IY44.
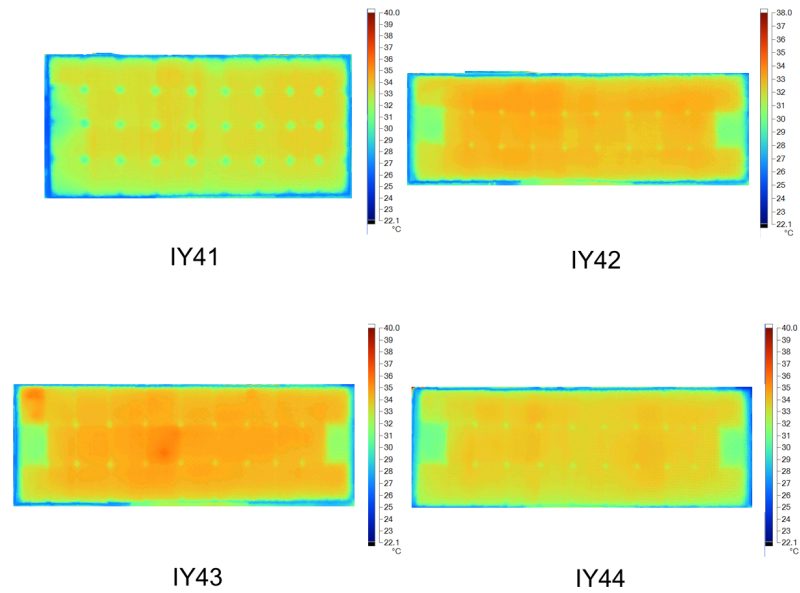

Figure 8: Infrared thermography under illumination for modules IY41, IY42, IY43 and IY44.
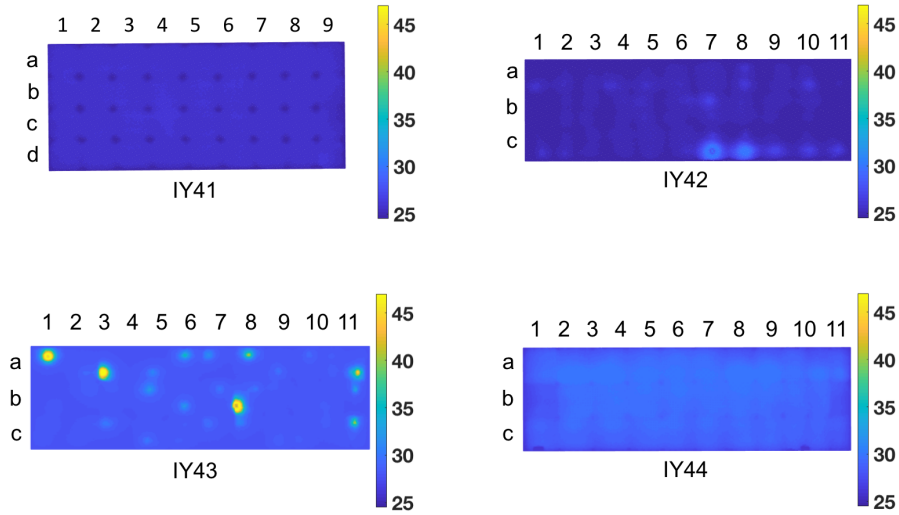
13

Figure 9: Thermal maps under dark condition for modules IY41, IY42, IY43 and IY44.

illuminated IR images display a much more uniform temperature distribution and concentrated defects are not detectable by a qualitative analysis (Fig. 10).

3.4. Quantitative statistical analysis of EL and IR images

Starting from the histograms, computed for each cell, we have evaluated the the behavior of the average value of maximum peak in the histograms for each defect class. Fig. 11 shows the average of the maximum (%) of histograms for EL (a), IR under biased condition (b) and illuminated condition (c) per each defect class. A slight overlap in red, green and blue channels is observable both in biased and illuminated condition. The maximum peak of green channel has a lower value respect to red and blue one for forward biased condition, but the same trends is not visible under illuminated condition. The maximum peak of EL signal floats around 10% and, considering the error bar, is not possible to denote a general trend related to the defects classes from the analysis of maximum.

Afterwards, the range of intensity for each defect class is calculated by averaging the intervals corresponding to all solar cells of the corresponding
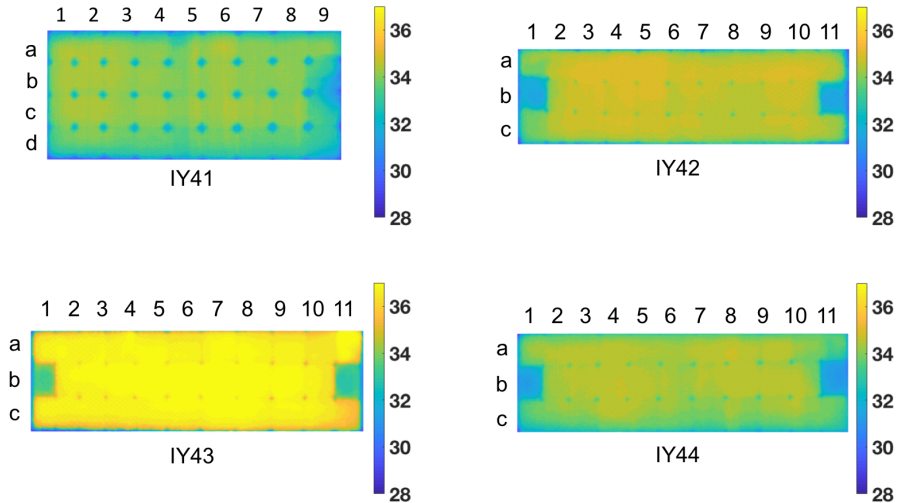
Figure 10: Thermal maps under illumination for modules IY41, IY42, IY43 and IY44.

defect class. Such a range depends both on the defect class and on module condition. The analysis of the EL signal shows an increasing trend in the range of intensities by moving from HC 2 up to SR (Fig. 12). Visual inspection seems to be required for a careful discrimination among different defect classes because of frequent overlapping between the intervals corresponding to different defect classes. We applied this approach to IR histograms under biased and illuminated condition.

Average x-range values for red, green and blue intensity are shown in Fig. 13 for biased condition and in Fig. 14 for illuminated condition. The order sequence adopted is the same chosen in Fig. 12.

For IR images under forward bias condition, the red and blue channels have an abrupt and opposite change in the ranges from the class DCI XXL 2 onwards. For defect classes from HC 2 up to DCI XXL 2, the range in in the interval between zero and 0.23. From DCI XXL 3 to the SR classes, on the other hand, the interval shifts in the range from 0.78 and unity. The opposite trend is observed for the blue channel, while the green channel has a trend similar to the red one, but without a sharp shift. Only the CC class (CC 1 for the red channel and CC 2 for the red and the blue channels) does not fulfill the observed trend, which can be motivated by the fact that the detected

15
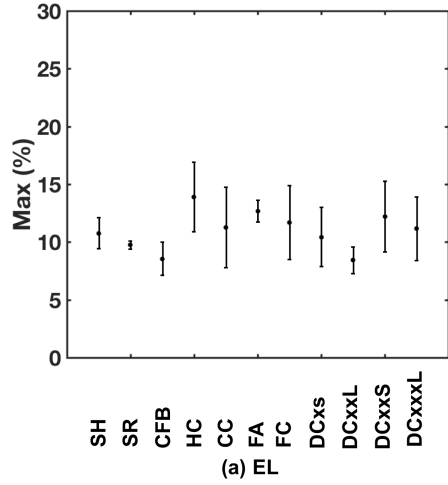
(a) EL
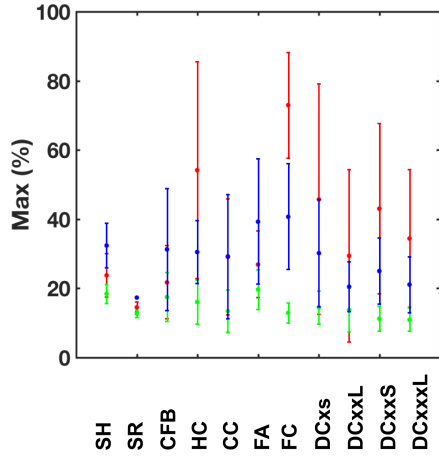
(b) IR forward bias
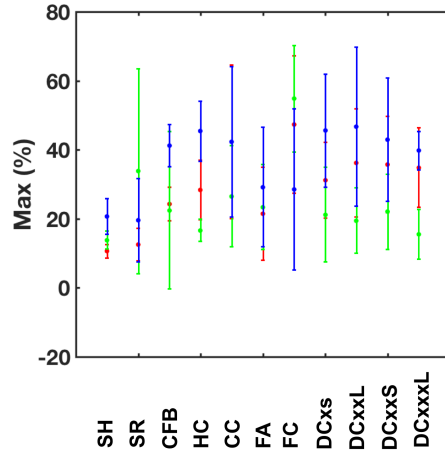
(c) IR illuminated

Figure 11: Average value of the absolute peak of the histogram of EL and IR signal per each defect class.

cross cracks are sources of minor defects for the examined cells. From the physical point of view, these results imply that it is possible to distinguish disconnected cell interconnect (DCI), humidity corrosion (HC) and finger interruption (FC) in highly damaged solar cells. The same analysis repeated
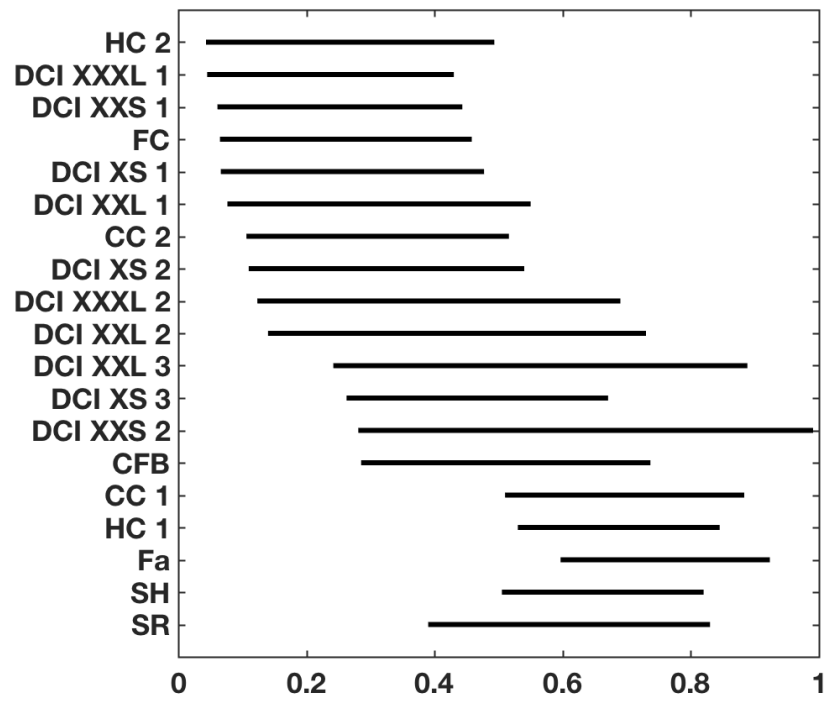
16

Figure 12: X-range of intensities histogram for EL signal for the different classes of defects in Fig.6.

Figure 13: X-range of intensities histogram for red, green and blue channels of the IR signal under forward bias condition, for the different classes of defects in Fig. 6.

for the histograms of the IR images taken under illumination (Fig. 14) do not show any shift in the interval ranges, thus making nearly impossible to distinguish between the different classes of defects.

4. Conclusions

We proposed a characterization of monocrystalline PV modules after 20 years of exposure and operation on a solar car and a statistical analysis of EL and IR under forward bias and illumination. The soiling effect, already visible from the visual characterization, has been confirmed by a $P_{\max}$ increase of 14% on average after a manual cleaning of the exposed modules, due to an increase of I_{sc}. One of the modules has presented a severe damage with a decrease of the FF below 37%. The annual degradation rate was -0.24% for the module on the bonnet and between -0.84 to -2.75% for the other
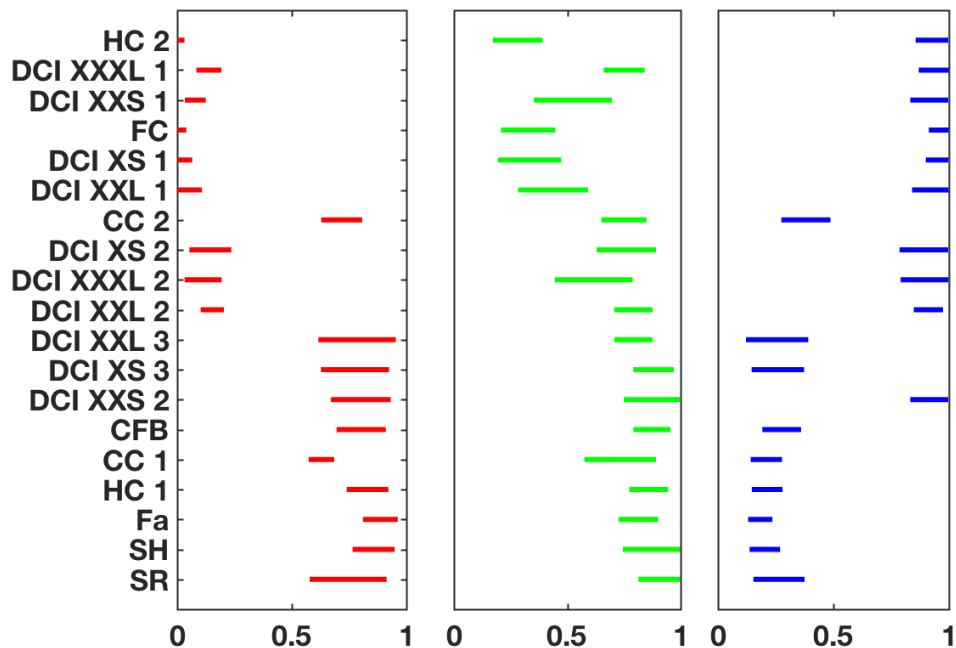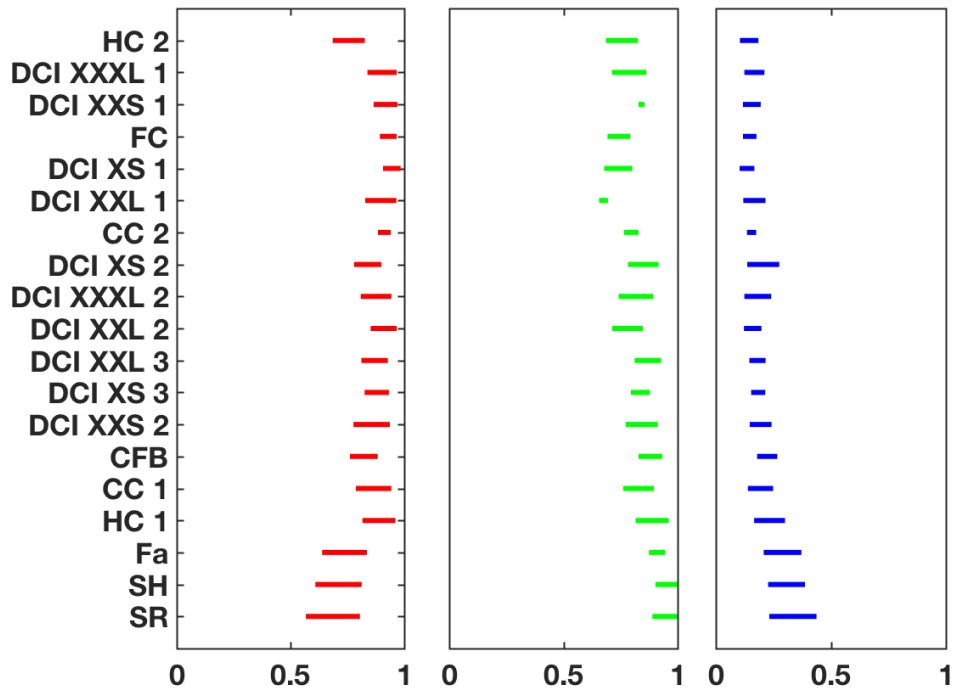
18

Figure 14: X-range of intensities histogram for red, green and blue channels of the IR signal under forward bias condition, for the different classes of defects in Fig. 6.

modules. Such degradation rates are slight higher than previously reported values (Jordan and Kurtz, 2013; Lopez et al., 2015; Jordan and Kurtz, 2016) and they seem to be depended both on the manufacturer and the mounting position.

The quantitative analysis proposed was an attempt to correlate EL and IR images from aged Pv modules to derive further information on the combined use of such two techniques. Starting from a visual inspection, we showed that most of the defects detected in IR images under forward bias are also visible in the EL images, also in monocrystalline silicon modules. Moreover, frequency histograms of the EL and R, G, B channel intensities, normalized in the range from zero to unity, provide useful indication of such defects and should be considered as a tool for a quantitative analyses. Indeed, the range of intensities in the frequency histograms can be correlated to the classes of defects for IR images taken in forward bias conditions. Particularly for the data herein analyzed, the range of intensities had an abrupt change of the range for red and blue channels towards higher intensities from defect classes DCI XXL2 to HC2, as compared to defect classes from SR to DCI XX3. Correspondingly, EL intensities had an increase. This confirms the qualitative relationship between EL and IR images under forward bias condition established for thin-film solar cells (see Zamini et al. (2012); Ebner et al. (2010, 2015b)), and it has been herein extended to monocrystalline solar cells for a wide range of defects. Future work might involve the implementation of the proposed statistical analysis in a machine learning algorithm, for real time identification of some classes of defects.

References

Bothe, K., Hinken, D., Ramspeck, K., Fischer, B., Brendel, R., 2007. Combined quantitative analysis of electroluminescence images and lbic mappings, in: Proc. 22nd European Photovoltaic Solar Energy Conference, Milan, Italy, p. 1673.

Bothe, K., Pohl, P., Schmidt, J., Weber, T., Altermatt, P., Fischer, B., Brendel, R., 2006. Electroluminescence imaging as an in-line characterisation tool for solar cell production, in: 21st European Photovoltaik Solae Energy Conference, Dresden, pp. 597–600.

Breitenstein, O., Bauer, J., Trupke, T., Bardos, R., 2008. On the detection of shunts in silicon solar cells by photo-and electroluminescence imaging. Progress in Photovoltaics: research and Applications 16, 325–330.

Buerhop, C., Schlegel, D., Vodermayer, C., Nieβ, M., 2011. Quality control of pv-modules in the field using infrared-thermography, in: 26th European Photovoltaic Solar Energy Conference, pp. 3894–3897.

Dolara, A., Lazaroiu, G., Leva, S., Manzolini, G., 2013. Experimental investigation of partial shading scenarios on PV (photovoltaic) modules. Energy 55, 466–475.

Ebner, R., Kubicek, B., Újvári, G., Berger, K., 2013. Non-destructive techniques for quality control of PV modules: infrared thermography, electro- and photoluminescence imaging, in: 39th Annual Conference of the IEEE Industrial Electronics Society, pp. 8104–8109.

Ebner, R., Kubicek, B., Újvári, G., Berger, K., 2015a. Optical characterization of different module technologies. Japanese Journal of Applied Physics 54, 08KG02.

Ebner, R., Kubicek, B., Újvári, G., Novalin, S., Rennhofer, M., Halwachs, M., 2015b. Optical characterization of different thin film module technologies. International Journal of Photoenergy , 159458.

Ebner, R., Zamini, S., Újvári, G., 2010. Defect analysis in different photovoltaic modules using electroluminescence (EL) and infrared (IR)-thermography. 25th EPVSEC, Valencia , 333.

Fuyuki, T., Kondo, H., Kaji, Y., Ogane, A., Takahashi, Y., 2007. Analytic findings in the electroluminescence characterization of crystalline silicon solar cells. Journal of Applied Physics 101, 023711.

Gade, V., Shiradkar, N., Paggi, M., Opalewski, J., 2015. Predicting the long term power loss from cell cracks in PV modules, in: Photovoltaic Specialist Conference (PVSC), 2015 IEEE 42nd, IEEE. pp. 1–6.

Haunschild, J., Glatthaar, M., Kasemann, M., Rein, S., Weber, E., 2009. Fast series resistance imaging for silicon solar cells using electroluminescence. physica status solidi (RRL)-Rapid Research Letters 3, 227–229.

Hinken, D., Ramspeck, K., Bothe, K., Fischer, B., Brendel, R., 2007. Series resistance imaging of solar cells by voltage dependent electroluminescence. Applied Physics Letters 91, 182104.

Jordan, D., Kurtz, S., 2013. Photovoltaic degradation rates - an analytical review. Progress in Photovoltaics: Research and Applications 21, 12–29.

Jordan, D., Kurtz, S., 2016. Compendium of photovoltaic degradation rates. Progress in Photovoltaics: Research and Applications 24, 978–989.

Koch, S., Weber, T., Sobottka, C., Fladung, A, e.a., 2016. Outdoor electroluminescence imaging of crystalline photovoltaic modules: comparative study between manual ground-level inspections and drone-based aerial surveys, in: 32nd European Photovoltaic Solar Energy Conf. and Exhibition, Munich Germany.

Köntges, M., Kunze, I., Kajari-Schröder, S., Breitenmoser, X., Bjørneklett, B., 2011. The risk of power loss in crystalline silicon based photovoltaic modules due to micro-cracks. Solar Energy Materials and Solar Cells 95, 1131–1137.

Köntges, M., Kurtz, S., Packard, C., Jahn, U., Berger, K., Kato, K., Friesen, T., Liu, H., Van Iseghem, M., 2014. Review of failures of photovoltaic modules. IEA PVPS Task 13.

Kropp, T., Berner, M., Stoicescu, L., Werner, J., 2017. Self-sourced daylight electroluminescence from photovoltaic modules. IEEE Journal of Photovoltaics 7, 1184–1189.

Lopez, J., Pozza, A., Sample, T., 2015. Analysis of crystalline silicon pv modules after 30 years of outdoor exposure. Proc. 31st EU PVSEC .

Lopez-Garcia, J., Pozza, A., Sample, T., 2015. Analysis of crystalline silicon pv modules after 30 years of outdoor exposure, in: 31th European Photovoltaic Solar Energy Conference and Exhibition, Hamburg, Germany, pp. 1847–1853.

Lopez-Garcia, J., Pozza, A., Sample, T., 2016. Long-term soiling of silicon pv modules in a moderate subtropical climate. Solar Energy 130, 174–183.

Mertens, K., K'osters, H., Diehl, M., 2015. Low-cost-outdoor-el: cost-efficient extensive on-site quality analysis of solar modules, in: Proceedings of the 31st European Photovoltaic Solar Energy Conference and Exhibition, 5BV.2.42, Hamburg, pp. 2300–2302.

Muehleisen, W., Eder, G., Voronko, Y., Spielberger, H., Sonnleitner, H., Knoebl, K., Ebner, R., Ujvari, G., Hirschl, C., 2018. Outdoor detection and visualization of hailstorm damages of photovoltaic plants. Renewable Energy 118, 138–145.

Paggi, M., Berardone, I., Infuso, A., Corrado, M., 2014. Fatigue degradation and electric recovery in silicon solar cells embedded in photovoltaic modules. Scientific Reports 4.

Paggi, M., Berardone, I., Martire, M., 2016. An electric model of cracked solar cells accounting for distributed damage caused by crack interaction. Energy Procedia 92, 576–584.

Schill, C., Brachmann, S., Heck, M., Weiss, K.A., Koehl, M., 2011. Impact of heavy soiling on the power output of pv modules, in: Proceedings of SPIE, p. 811207.

Schill, C., Brachmann, S., Koehl, M., 2015. Impact of soiling on IV-curves and efficiency of PV-modules. Solar Energy 112, 259–262.

Strahler, A., Strahler, A., Barrutia, M., Sunyer, P., 1981. Geografía física. Omega.

Würfel, P., Trupke, T., Puzzer, T., Schäffer, E., Warta, W., Glunz, S., 2007. Diffusion lengths of silicon solar cells from luminescence images. Journal of Applied Physics 101, 123110.

Zamini, S., Ebner, R., Újvári, G., Kubicek, B., 2012. Non-destructive-techniques for quality control of photovoltaic modules: electroluminescence imaging and infrared thermography. Photovoltaics International Journal, PV-Tech PRO , 127–203.